Chemical Science

ROYAL SOCIETY OF CHEMISTRY

EDGE ARTICLE

View Article Online
View Journal | View Issue

Cite this: *Chem. Sci.*, 2024, **15**, 18846

All publication charges for this article have been paid for by the Royal Society of Chemistry

Received 10th August 2024
Accepted 22nd October 2024

DOI: 10.1039/d4sc05374e

rsc.li/chemical-science

Large and long-term photon energy storage in diazetidines *via* [2+2] photocycloaddition†

Han P. Q. Nguyen, Anurag Mukherjee, Junichi Usuba, Joshua Wan and Grace G. D. Han *

We report a series of *p*-functionalized phenylbenzoxazoles that offer remarkable energy storage, exceeding 300 J g^{-1}, for the first time among intermolecular cycloaddition-based molecular solar thermal energy storage systems. The [2 + 2] photocycloaddition of phenylbenzoxazoles generates diazetidine cycloadducts that store energy for up to 23 years in the solid state and release energy upon triggered cycloreversion. The solid-state phase transition contributes to increasing overall energy storage densities, and the dearomative cycloaddition process is revealed to be critical for maximizing the intrinsic energy storage capacities. The solvent-assisted cycloreversion is also used to accelerate the energy release from the emerging molecular scaffold.

Introduction

The concept of molecular solar thermal (MOST) energy storage has been largely demonstrated using photoswitches that undergo either *E*–*Z* isomerization or intramolecular cycloadditions, with examples including azo(hetero)arenes,[1–4] hydrazones,[5] dihydroazulenes,[6,7] fulvalene diruthenium[8,9] derivatives, and norbornadienes.[10,11] In particular, norbornadienes that undergo intramolecular [2 + 2] photocycloaddition to generate quadricyclanes have been recognized for storing a large quantity of energy over 300 J g^{-1},[12,13] primarily in the solution state. A quadricyclane bearing a four-membered ring is highly strained and thus destabilized, which rationalizes a large energy difference between a thermodynamically-stable norbornadiene and its cycloadduct, quadricyclane. Additionally, the intramolecular [2 + 2] cycloadditions in molecular scaffolds beyond norbornadienes have been rigorously investigated for MOST energy storage, including many bicyclic dienes[14] such as bicyclooctadienes.[15] Significant effort has also been devoted to identifying potential intramolecular switchable systems with favorable parameters for energy storage, such as optimal light absorption ranges,[16–19] enhanced fatigue resistances,[20–22] prolonged thermal half-lives,[23–26] diverse switching mechanisms,[27,28] and high quantum yields of photoisomerization.[29–33] In contrast, energy storage capitalizing on intermolecular photocycloaddition reactions[34–36] remains relatively underexplored, which opens up new opportunities to harness the potential of a wide range of photochemistry.

For example, a class of solid-state MOST compounds has recently emerged, storing photon energy *via* crystalline-state intermolecular photochemical reactions, as seen in the [2 + 2] photocycloaddition of styrylpyryliums[37] and [4 + 4] photocycloaddition of anthracenes.[38] These systems exhibit thermally activated cycloreversion in the solid state, which improves the gravimetric density of the released energy in the absence of solvents. However, the reported cycloaddition-based MOST systems present intrinsically suboptimal energy storage capacity. A maximum energy storage density ($\Delta H_{storage}$) of 42 kJ mol^{-1} (51 J g^{-1}) was achieved for styrylpyryliums,[37] which is substantially lower than the average $\Delta H_{storage}$ values of photoswitches – over 100 kJ mol^{-1} and 300 J g^{-1} for conventional MOST systems such as azo(hetero)arenes[39–41] and norbornadienes.[42,43] Donor–acceptor substituted anthracenes offer larger $\Delta H_{storage}$ up to 96 kJ mol^{-1} or 221 J g^{-1},[38] while they have not matched the capacities of traditional photoswitches. Moreover, their cycloadducts, *i.e.*, dianthracenes, reported rather short half-lives of 1–6 days, which makes them suboptimal for long-term energy storage.

Thus, it has been a challenging quest to discover an intermolecular cycloaddition reaction that allows for enhanced and long-term energy storage in cycloadducts even at elevated temperatures. To improve $\Delta H_{storage}$, it is necessary to destabilize the metastable cycloadducts, and heteroatom substitution to the strained rings would be a potential strategy for fine-tuning the stability of the rings. A theoretical study estimates that substituting a cyclobutane with one nitrogen atom slightly lowers the strain energy of the azetidine ring (106 kJ mol^{-1}) compared to cyclobutane (110 kJ mol^{-1}).[44] On the other hand, the ring strain of a 1,3-diazetidine, a four-membered ring composed alternatively of C and N atoms, is predicted to be significantly larger (128 kJ mol^{-1}), which makes the diazetidine

Department of Chemistry, Brandeis University, 415 South Street, Waltham, MA 02453, USA. E-mail: gracehan@brandeis.edu

† Electronic supplementary information (ESI) available. See DOI: https://doi.org/10.1039/d4sc05374e

a desirable MOST energy storage compound. Furthermore, the formation of 1,3-diazetidines can be induced *via* [2 + 2] cycloadditions of C=N bonds,[45] and they have been reported to undergo thermally activated cycloreversion in solutions.[46–48]

However, the MOST energy storage potential of diazetidines has been rarely investigated, presumably because of the relative scarcity of [2 + 2] C=N bond photocycloaddition processes and the predominant research effort emphasized on their use in synthetic procedures.[49–51] To date, there is only one report that evaluated the exotherm of acid-catalyzed reversion of a diazetidine in solution (116 kJ mol^{-1}) by Paillous and co-workers in 1982.[48] Nonetheless, the use of acid hinders further cycloaddition of phenylbenzoxazoles, limiting the use of the scaffold for energy storage. Follow-up studies in 1986 and 1987 reported the photodimerization and dehalogenation of 2-(4-halophenyl) benzoxazoles, as well as solution-state cycloreversion of two diazetidines.[52,53] Independently, Mohr and co-workers discovered the solid-state dimerization of oxazolones and solution-state acid-catalyzed cycloreversion of their diazetidine dimers in 1984.[54] Yet, in these early studies, the potential of diazetidines for photon energy storage remained unexplored; none of their energy storage densities, durations, cyclabilities, solid-state energy storage capabilities, or solid-state energy release characteristics were known.

Herein, we unravel the [2 + 2] cycloaddition and reversion processes of phenylbenzoxazole/diazetidine and report design principles for achieving exceptionally large energy storage densities and long energy storage times in the solid state, now on par with state-of-the-art photoswitches. Additionally, we unveil solvent-assisted cycloreversion of diazetidines, which employs a minimal amount of solvent instead of acid to facilitate efficient energy release under mild temperature conditions.

Results and discussion

We inspected a series of *p*-functionalized phenylbenzoxazole (PB) derivatives that undergo light-induced [2 + 2] cycloadditions to form diazetidine (DA) moieties (Fig. 1a). The DAs can be thermally activated to revert to PBs, releasing the stored energy ($\Delta H_{storage}$) as heat. The functional groups were varied to test their inductive effect on energy storage: H (**1**), F (**2**), Cl (**3**), and Me (**4**) (Fig. 1b). In addition, the varied functional groups effectively control the melting points of PBs, which allows for decoupling the exothermic cycloreversion of DAs and endothermic melting of PBs. Any overlap between these two processes results in reduced overall energy release (*vide infra*), which can be averted by judicious molecular designs.

PBs and corresponding DAs exhibit intrinsically overlapping absorption in the UV range (Fig. 1c and S1†), which limits the effective UV-induced [2 + 2] cycloaddition either in solid or in solution. Furthermore, *p*-functionalized PBs predominantly exhibit photoluminescence in solid.[55,56] To overcome the challenge, we performed the irradiation of PBs under hexane/water biphasic conditions where PBs are dissolved in the hexane layer (Fig. 1d).[53,57] The hexane/water interface facilitates the precipitation of the formed DA cycloadducts by anchoring them and allowing them to grow into bigger solid particles. The DA solids are less prone to undergo UV-induced [2 + 2] cycloreversion, which in turn resulted in 70–90% yield of cycloaddition in 3 days. Achieving similar yields required longer reaction time under single-phase solution-state reaction conditions such as in pure hexane (Table S1†). The quantum yield of PB cycloaddition is also reported to increase significantly under biphasic conditions in previous studies.[52,53] The 2PB → DA conversion is confirmed by solution-state nuclear magnetic resonance (NMR) spectroscopy and Fourier-transform infrared (FT-IR) spectroscopy (Fig. S2–S23†). We have additionally attempted the dimerization of PBs with *p*-CN and *p*-OMe functional groups among others in various solvents. However, the compounds with strong electron-donating and -withdrawing substituents did not result in the formation of stable dimers, which could be attributed to the facile cycloreversion of DAs in solutions.

Heat release from the collected DAs was investigated using differential scanning calorimetry (DSC) (Fig. 2a and b). For compound **3** with a *p*-Cl substituent, DA → 2PB cycloreversion was observed upon heating, releasing $\Delta H_{storage}$, followed by the sharp melting transition of the generated PB-**3** (Fig. 2a). The

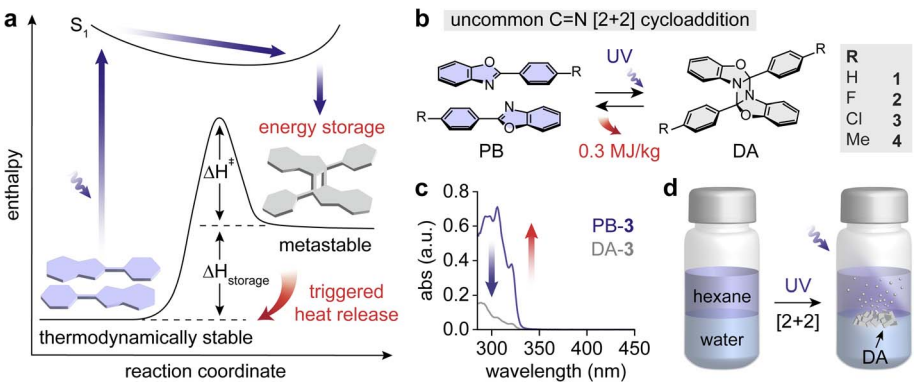

Fig. 1 (a) An energy diagram illustrating solar photon energy storage through [2 + 2] cycloaddition of phenylbenzoxazole (PB) and energy release by triggered cycloreversion of diazetidine (DA). (b) Reversible photo-induced [2 + 2] cycloaddition and thermal reversion between PB and DA derivatives **1**–**4**. (c) Solution-state UV-vis absorption spectra of PB-**3** and DA-**3** in toluene. (d) Schematic illustration of the photo-cycloaddition setup: hexane/water biphasic solution under oxygen-free conditions.

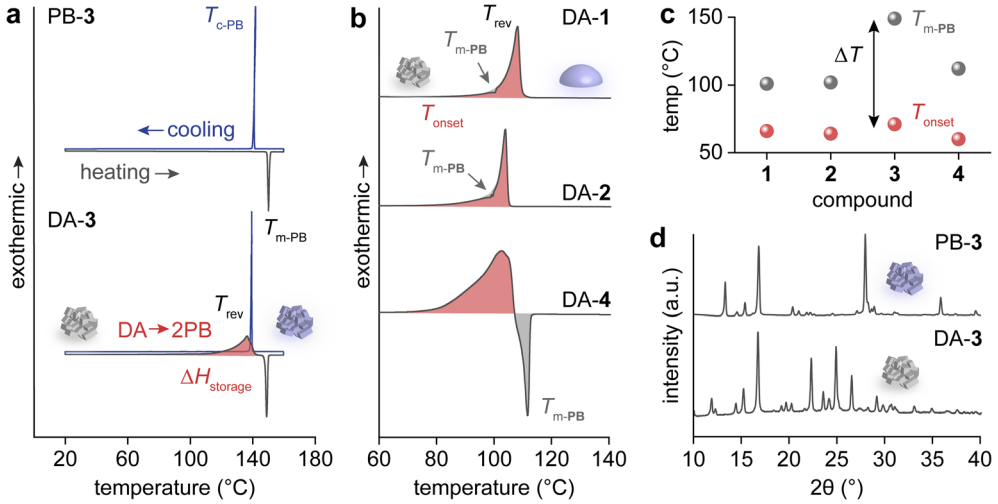

Fig. 2 (a) DSC thermograms of PB-**3** and DA-**3** measured during the first heating (black) and cooling (blue) cycle. (b) DSC thermograms of DA-**1**, DA-**2**, and DA-**4**, measured during the first heating cycle. (c) Relative $T_{m\text{-}PB}$ and T_{onset} of compounds **1**–**4**. (d) PXRD patterns of PB-**3** and DA-**3**. Red highlighted areas represent the exotherms of cycloreversion ($\Delta H_{storage}$). Grey highlighted areas represent the endotherms of melting of phenylbenzoxazole; $T_{m\text{-}PB}$, melting point of phenylbenzoxazole; $T_{c\text{-}PB}$, crystallization point of phenylbenzoxazole; T_{rev}, peak temperature of thermal reversion; T_{onset}, onset temperature of thermal reversion; ΔT, difference between $T_{m\text{-}PB}$ and T_{onset}.

molten PB-**3** crystalizes when cooled, identical to the pristine PB-**3**'s melting and crystallization behaviors, which confirms the generation of PB-**3** from DA-**3**'s cycloreversion. In particular, the formation of crystalline-state PB indicates the nature of the solid-to-solid transition of the DA → 2PB reaction.

Similarly, the heating curves of DAs **1**, **2**, and **4** show exothermic cycloreversion, while the simultaneous cycloreversion and melting of PBs results in a reduced overall exotherm (*i.e.*, integrated area of the exothermic peak, highlighted in red) (Fig. 2b). The melting points of PBs **1**, **2**, and **4** ($T_{m\text{-}PB}$) are 101 °C, 102 °C, and 112 °C, respectively, much lower than that of PB-**3** at 149 °C (Fig. 2c and S24†). A large temperature gap (ΔT) between $T_{m\text{-}PB}$ (marked in grey) and the onset of DA's reversion (T_{onset}, marked in red) over 78 °C is necessary for the complete solid-to-solid cycloreversion and heat release, as observed for compound **3**. The powder X-ray diffraction (PXRD) of PB-**3** and DA-**3** confirms the crystalline nature of both compounds (Fig. 2d). Because of the smaller ΔT values for **1**, **2**, and **4** (35 °C, 38 °C, and 52 °C, respectively), their heat release was compromised by the subsequent melting of PBs, limiting the $\Delta H_{storage}$ values to 256–280 J g^{-1}. In contrast, compound **3** shows the largest $\Delta H_{storage}$ value of 318 J g^{-1} among all compounds (Table 1). The photon energy storage and subsequent heat release of the PB/DA system are also repeatable. We conducted a cycling test for compound **1** with repeated 300 nm irradiation and 15-minute thermal activation at 110 °C. The solubility of PB-**1** gradually decreased over the repeated cycloaddition and cycloreversion, which slightly lowered the conversion of PB-**1** after the 2nd cycle. However, no degradation was detected by NMR over 5 cycles, confirming the system's stability and cyclability (Fig. S25 and S26†).

These different heat release processes observed between DA-**3** and other DAs **1**, **2**, and **4** were rigorously compared using an isothermal DSC, and the kinetics of condensed-phase exothermic cycloreversion reactions were analyzed. The cycloreversion of DA-**3** was monitored at 105 °C, which clearly showed a gradual increase in heat release over time that peaks and decays after 3 hours of the isothermal reaction (Fig. 3a). The

Table 1 Thermal parameters for the cycloreversion process[a]

		Solid-state				Solvated-state		
Cycloreversion	$T_{m\text{-}PB}$ (monomer)	T_{onset} (°C)	ΔT (°C)	$\Delta H_{storage}$ (kJ mol^{-1})	$\Delta H_{storage}$ (J g^{-1})	T_{onset} (°C)	$\Delta H_{storage}$ (kJ mol^{-1})	$\Delta H_{storage}$ (J g^{-1})
1	101	66	35	101	260	39	108	277
2	102	64	38	109	256	30	133	312
3	149	71	78	146	318	34	109	237
4	112	60	52	117	280	23	94	224
Styrylpyrylium	250	132	118	42	51	n/a	n/a	n/a
Anthracene	197	59	138	102	195	n/a	n/a	n/a

[a] $T_{m\text{-}PB}$, melting point of the phenylbenzoxazole monomer; T_{onset}, onset temperature of cycloreversion; $\Delta H_{storage}$, energy storage density; ΔT, difference between $T_{m\text{-}PB}$ and T_{onset}.

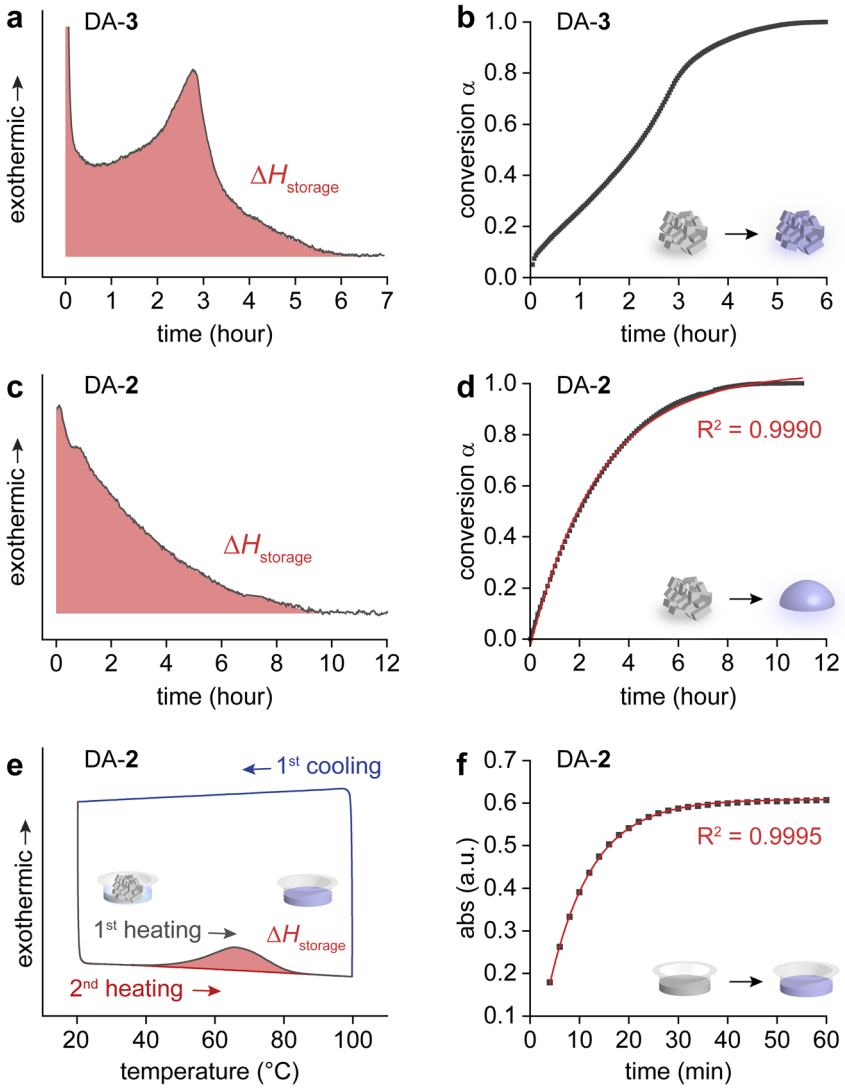

Fig. 3 (a) A DSC thermogram of DA-**3** measured at 105 °C. (b) Conversion of DA-**3** over time at 105 °C. (c) A DSC thermogram of DA-**2** measured at 80 °C. (d) Conversion of DA-**2** over time at 80 °C. (e) A DSC thermogram of DA-**2** solvated by toluene during the first (black) and second heating (red) and the first cooling (blue) cycle. (f) Conversion of DA-**2** over time in toluene at 70 °C. Red highlighted areas represent $\Delta H_{storage}$. The R^2 values are for the red curves fitted for 1st-order kinetics.

conversion (α) of DA-**3** over time indicates an autocatalytic process, displaying a sigmoidal function with a very short induction period (Fig. 3b). Other solid-state reactions including [3 + 2] thermal cycloadditions[58] and [2 + 2][59] or [4 + 4] photodimerizations[60–62] have been reported to show autocatalysis, which is attributed to the molecular cooperativity in the crystalline-state reactions. Thus, we hypothesize that DA → 2PB cycloreversion occurring in the solid state also undergoes a cooperative autocatalytic process. In contrast, the isothermal DSC measurement of DA-**2** at 80 °C primarily displayed a decaying exothermicity (Fig. 3c) and decelerating reaction rate over time (Fig. 3d). The isothermal DSC and kinetic analysis of DA-**1** and DA-**4** were similar to those of DA-**2** (Fig. S27–S32†). The 1st-order kinetics found in the cycloreversion of DAs **1**, **2**, and **4** indicate that the reactions likely proceed in disordered phases, which is supported by the simultaneous cycloreversion of DAs and melting of resulting PBs (Fig. 2b). Thus, not only the degree of heat release but also its kinetics are revealed to largely depend on the molecular designs and their phase transition during the condensed-phase cycloreversion.

To examine pristine $\Delta H_{storage}$ values of all compounds, we employed solvation that circumvents the unfavorable melting of PBs that are generated upon cycloreversion. A small amount of toluene (25 μL) was added to DAs (0.6 mg) at room temperature, and the mixture was heated to induce a DA → 2PB reaction, as evidenced by the broad exotherm in Fig. 3e. For compounds **1**–**2** experiencing a complete overlap of the cycloreversion and melting transitions, the measured $\Delta H_{storage}$ significantly increased in the solvated state (Table 1). In contrast, $\Delta H_{storage}$ values were larger in the solid state than in the solvated state for compounds **3**–**4** for which the cycloreversion and melting are either partially or completely resolved. This suggests that the exothermic solid-to-solid phase transition of DA → 2PB cycloreversion contributes to the overall heat release of compounds

3–4, whereas the melting event undermined the heat release of compounds **1–2**. It is worth noting that the solvation energy of PB generated upon cycloreversion in toluene is negligible at the experimental concentration (Fig. S33†). When the PB concentration was increased by 2.5 fold, a broad endothermic peak was observed with an integrated value of 3 J g^{-1}, suggesting a minor endothermic effect even at higher concentrations. The thermogravimetric analysis (TGA) (Fig. S34†) and solution-state DSC measurements of all compounds are shown in Fig. S35,† and the NMR spectra of the restored PBs after DSC are shown in Fig. S36–S39.† The 1st-order kinetics of solution-state cycloreversion for all compounds were observed by the analysis of their UV-vis absorption changes (Fig. 3f, S40–S43†).

The markedly lower T_{onset} (below 40 °C) for cycloreversion of DAs in toluene, compared to those in the solid state (Table 1), suggests that solvation also lowers the activation energy for thermal cycloreversion. This reduction is attributed to the loss of intermolecular interactions in the crystalline state upon solvation, which allows for a more facile cycloreversion of DA species. Our DFT calculations also suggest that the stabilization of the polarized transition state using solvents with high dielectric constants further contributes to the acceleration of the cycloreversion process in solutions (Fig. S44†, Tables S2–S5†). Our measurement of the enthalpy of activation ($\Delta H^{\ddagger}$) of cycloreversion corroborates this finding (Table 2). The $\Delta H^{\ddagger}$ and half-life ($t_{1/2}$) of DA's cycloreversion were characterized in both solid and solution states using DSC and UV-vis spectroscopy. Notably, solid-state DAs exhibit exceptionally long thermal $t_{1/2}$ (ranging from days to 23 years), highlighting the potential for stable energy storage for years even at elevated temperatures. Remarkably, the $t_{1/2}$ of DAs reduces to hours in toluene, making solvent-assisted cycloreversion a viable option. Solvation-catalyzed cycloreversion is more favorable for repeating MOST energy storage and release cycles, compared to the reported acid-catalyzed reversion method that requires the removal of acid before the next cycle of photo-cycloaddition. Thus, the solvation method is effective for maximizing and accelerating energy release from low-melting PBs at temperatures below 40 °C.

Table 1 summarizes the critical thermal parameters relevant to the cycloreversion of DAs **1–4** in both solid and solvated states. It also lists the metrics of a styrylpyrylium and an anthracene derivative that has exhibited the largest energy storage among cycloaddition-based solid-state MOST systems reported so far. Compounds **1–4** demonstrate substantial $\Delta H_{storage}$, both per molecule and per gram, comparable to those of norbornadienes[42,43] and phase-transition MOST compounds based on azo(hetero)arenes.[39–41] These values reach up to 146 kJ mol^{-1} or 318 J g^{-1}, significantly surpassing those of styrylpyryliums (max 42 kJ mol^{-1} or 51 J g^{-1}) and anthracenes (max 102 kJ mol^{-1} or 195 J g^{-1}). The PB-**3**/DA-**3** pair therefore offers the highest energy storage density among all reported solid-state MOST systems utilizing intermolecular cycloadditions (Table S6†).

The moderate electronic effect of functional groups on energy storage can be investigated by comparing the $\Delta H_{storage}$ values measured in the solvated-state (Table 1), which excludes the impact of the solid-to-solid phase transition or melting on the DSC measurements. Electron-withdrawing groups are hypothesized to reduce the electron density of the C–N bonds on a DA ring, destabilizing the metastable photodimer. This in turn may increase the energy gap between PB and DA, resulting in the largest $\Delta H_{storage}$ value of 133 kJ mol^{-1} for DA-**2** with a *p*-F functional group. On the other hand, electron-donating groups such as a *p*-Me group of DA-**4** may increase the electron density of the DA ring *via* a modest inductive effect. The dimer is relatively stabilized, which causes a smaller energy difference between PB-**4** and DA-**4**, leading to the lowest $\Delta H_{storage}$ value of 94 kJ mol^{-1} for DA-**4**.

Lastly, we performed a theoretical investigation, surveying the role of dearomative cycloaddition in achieving substantial energy storage densities. We first analyzed the aromaticity change of each ring in the molecular structure of PB before and after cycloaddition using nucleus-independent chemical shift (NICS)[63] indices (Fig. 4a). According to the chemical structure changes, a prominent loss of aromaticity is expected for PB-**1** upon its dimerization (Fig. 4b). In contrast, the aromaticity changes in phenyl-3*H*-indole upon cycloaddition would be insignificant, due to its non-aromatic central ring (B) (Fig. 4c). The dimerization of phenylbenzofuran would yield an aromaticity loss similarly to phenylbenzoxazole (Fig. 4d). These predictions are supported by the calculated NICS values; while the aromaticity of the outer two rings (A and C) remains nearly intact after dimerization, the most notable changes in aromaticity are found in the central ring B for PB-**1** and phenylbenzofuran (Fig. 4e). The dearomative cycloaddition of PB-**1** can rationalize the larger energy difference between PB and DA (ΔH_{calc} of 104 kJ mol^{-1}) compared to a ΔH_{calc} of 25 kJ mol^{-1} for phenyl-3*H*-indole that does not undergo dearomatization. Despite the significant dearomatization of phenylbenzofuran, its ΔH_{calc} is also small, which is attributed to the formation of a cyclobutane ring

Table 2 Eyring activation energy parameters and the extrapolated half-lives at 298 K of DAs **1–4**[a]

	Solid-state				Solvated-state			
DA → PB	$\Delta G^{\ddagger}$ (kJ mol^{-1})	$\Delta H^{\ddagger}$ (kJ mol^{-1})	$\Delta S^{\ddagger}$ (kJ mol^{-1})	$t_{1/2}$ (days)	$\Delta G^{\ddagger}$ (kJ mol^{-1})	$\Delta H^{\ddagger}$ (kJ mol^{-1})	$\Delta S^{\ddagger}$ (kJ mol^{-1})	$t_{1/2}$ (hours)
1	117	121	0.013	306	100	85	−0.049	8.8
2	115	116	0.004	135	97	63	−0.114	3.4
3	125	131	0.021	8372	98	74	−0.081	5.3
4	118	154	0.122	642	97	69	−0.093	3.1

[a] $\Delta G^{\ddagger}$, Gibbs free energy of activation; $\Delta H^{\ddagger}$, enthalpy of activation; $\Delta S^{\ddagger}$, entropy of activation; $t_{1/2}$, extrapolated half-life of DA at 298 K.

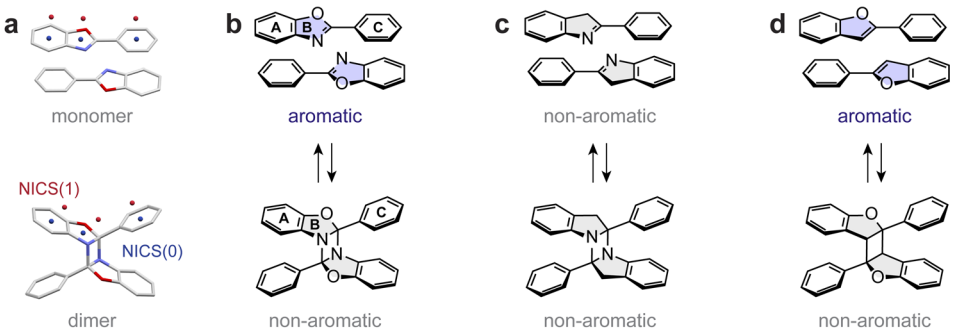

e		phenylbenzoxazole			phenyl-3*H*-indole			phenylbenzofuran		
	ring	A	B	C	A	B	C	A	B	C
monomer	NICS(1)	-12.2	**-7.9**	-13.2	-12.2	-3.4	-12.1	-13.1	**-8.2**	-12.1
	NICS(0)	-10.7	**-8.0**	-13.2	-11.3	+1.8	-10.5	-11.0	**-9.5**	-10.6
dimer	NICS(1)	-12.7	-2.6	-13.1	-12.8	-3.3	-13.1	-12.4	-2.2	-13.1
	NICS(0)	-13.1	-3.3	-11.7	-12.2	-1.9	-11.7	-12.1	-2.4	-11.7
	ΔH_{calc}	104			25			10		(kJ/mol)

Fig. 4 (a) Schematic illustration of NICS calculations, with NICS(0) calculated at the center of each ring and NICS(1) calculated at 1.0 Å above the plane of the ring. Reversible [2 + 2] dimerization of (b) phenylbenzoxazole, (c) phenyl-3*H*-indole, and (d) phenylbenzofuran. The aromatic *vs.* non-aromatic characters of the highlighted rings are labeled. (e) A table summarizing the calculated NICS(0) and NICS(1) values (HF/6-31G** level of theory) and energy storage density (ΔH_{calc}) of each cycloaddition system (B3LYP-D3/6-31G** level of theory). The coordinates of all optimized structures are included in Fig. S45, Tables S7–S12.†

that is not as strained as diazetidine.[44] Therefore, we conclude that both dearomative cycloaddition and the formation of largely strained cycloadducts are crucial design principles for reaching significant MOST energy storage over 300 J g^{-1}.

Conclusions

In summary, we discovered the design principles of diazetidine-based MOST systems that showcase exceptional energy storage densities, surpassing 300 J g^{-1}, far exceeding the reported values of recently discovered styrylpyryliums or anthracenes. Our study shows that these systems are well-suited for long-term energy storage, with half-lives up to 23 years, while enabling solvent-assisted energy release within hours at room temperature. The incorporation of heteroatoms into cyclic rings and the use of dearomative cycloaddition strategies were demonstrated to be crucial in enhancing the system performance. These insights provide a strong foundation for designing future photo-cycloaddition MOST systems and offer practical guidance for developing efficient, high-capacity energy storage solutions.

Data availability

The data supporting this article have been included as part of the ESI.†

Author contributions

H. P. Q. N. performed the synthesis of compounds **1–3**, DSC analyses, UV-vis spectroscopy, and PXRD measurements. A. M. synthesized compound **4** and characterized it. J. U. conducted DFT calculations. J. W. performed the preliminary studies on compounds **1–3**. G. G. D. H. conceived the project and refined the manuscript. All authors discussed the results and edited the manuscript.

Conflicts of interest

There are no conflicts to declare.

Acknowledgements

This material is based upon work supported by the Air Force Office of Scientific Research under Award Number FA9550-22-1-0254. G. G. D. H. acknowledges the NSF CAREER award (DMR-2142887), the Alfred P. Sloan Foundation (FG-2022-18328), and the Camille and Henry Dreyfus Foundation (TC-23-028). A. M. and J. W. were partly supported by Brandeis MRSEC (DMR-2011846). PXRD patterns were obtained on a powder X-ray diffractometer funded by AFOSR DURIP award (FA9550-23-1-0072). The solution-state NMR spectrometer used in this project was funded by the NIH Shared Instrumentation Program (1S10OD034395). We appreciate Ryo Koibuchi at the University of Tokyo for helpful discussions and insights on the monomer packing and lattice energy.

References

1 A. Kunz, A. H. Heindl, A. Dreos, Z. Wang, K. Moth-Poulsen, J. Becker and H. A. Wegner, Intermolecular London Dispersion Interactions of Azobenzene Switches for Tuning

Molecular Solar Thermal Energy Storage Systems, *ChemPlusChem*, 2019, **84**, 1145–1148.

2 M. Le and G. G. D. Han, Stimuli-Responsive Organic Phase Change Materials: Molecular Designs and Applications in Energy Storage, *Acc. Mater. Res.*, 2022, **3**, 634–643.

3 Z. Wang, R. Losantos, D. Sampedro, M.-A. Morikawa, K. Börjesson, N. Kimizuka and K. Moth-Poulsen, Demonstration of an azobenzene derivative based solar thermal energy storage system, *J. Mater. Chem. A*, 2019, **7**, 15042–15047.

4 L. Dong, Y. Feng, L. Wang and W. Feng, Azobenzene-based solar thermal fuels: design, properties, and applications, *Chem. Soc. Rev.*, 2018, **47**, 7339–7368.

5 Q. Qiu, S. Yang, M. A. Gerkman, H. Fu, I. Aprahamian and G. G. D. Han, Photon Energy Storage in Strained Cyclic Hydrazones: Emerging Molecular Solar Thermal Energy Storage Compounds, *J. Am. Chem. Soc.*, 2022, **144**, 12627–12631.

6 Z. Wang, J. Udmark, K. Börjesson, R. Rodrigues, A. Roffey, M. Abrahamsson, M. B. Nielsen and K. Moth-Poulsen, Evaluating Dihydroazulene/Vinylheptafulvene Photoswitches for Solar Energy Storage Applications, *ChemSusChem*, 2017, **10**, 3049–3055.

7 M. Brøndsted Nielsen, N. Ree, K. V. Mikkelsen and M. Cacciarini, Tuning the dihydroazulene – vinylheptafulvene couple for storage of solar energy, *Russ. Chem. Rev.*, 2020, **89**, 573.

8 Y. Kanai, V. Srinivasan, S. K. Meier, K. P. C. Vollhardt and J. C. Grossman, Mechanism of Thermal Reversal of the (Fulvalene)tetracarbonyldiruthenium Photoisomerization: Toward Molecular Solar–Thermal Energy Storage, *Angew. Chem., Int. Ed.*, 2010, **49**, 8926–8929.

9 A. Lennartson, A. Lundin, K. Börjesson, V. Gray and K. Moth-Poulsen, Tuning the photochemical properties of the fulvalene-tetracarbonyl-diruthenium system, *Dalton Trans.*, 2016, **45**, 8740–8744.

10 J. Orrego-Hernández, A. Dreos and K. Moth-Poulsen, Engineering of Norbornadiene/Quadricyclane Photoswitches for Molecular Solar Thermal Energy Storage Applications, *Acc. Chem. Res.*, 2020, **53**, 1478–1487.

11 K. Jorner, A. Dreos, R. Emanuelsson, O. El Bakouri, I. F. Galván, K. Börjesson, F. Feixas, R. Lindh, B. Zietz, K. Moth-Poulsen and H. Ottosson, Unraveling factors leading to efficient norbornadiene–quadricyclane molecular solar-thermal energy storage systems, *J. Mater. Chem.*, 2017, **5**, 12369–12378.

12 R. Schulte, S. Afflerbach, T. Paululat and H. Ihmels, Bis- and Tris-norbornadienes with High Energy Densities for Efficient Molecular Solar Thermal Energy Storage, *Angew. Chem., Int. Ed.*, 2023, **62**, e202309544.

13 Z. Wang, A. Roffey, R. Losantos, A. Lennartson, M. Jevric, A. U. Petersen, M. Quant, A. Dreos, X. Wen, D. Sampedro, K. Börjesson and K. Moth-Poulsen, Macroscopic heat release in a molecular solar thermal energy storage system, *Energy Environ. Sci.*, 2019, **12**, 187–193.

14 A. E. Hillers-Bendtsen, J. L. Elholm, O. B. Obel, H. Hölzel, K. Moth-Poulsen and K. V. Mikkelsen, Searching the Chemical Space of Bicyclic Dienes for Molecular Solar Thermal Energy Storage Candidates, *Angew. Chem., Int. Ed.*, 2023, **62**, e202309543.

15 M. Quant, A. E. Hillers-Bendtsen, S. Ghasemi, M. Erdelyi, Z. Wang, L. M. Muhammad, N. Kann, K. V. Mikkelsen and K. Moth-Poulsen, Synthesis, characterization and computational evaluation of bicyclooctadienes towards molecular solar thermal energy storage, *Chem. Sci.*, 2022, **13**, 834–841.

16 S. Helmy, S. Oh, F. A. Leibfarth, C. J. Hawker and J. Read de Alaniz, Design and Synthesis of Donor–Acceptor Stenhouse Adducts: A Visible Light Photoswitch Derived from Furfural, *J. Org. Chem.*, 2014, **79**, 11316–11329.

17 S. Helmy, F. A. Leibfarth, S. Oh, J. E. Poelma, C. J. Hawker and J. Read de Alaniz, Photoswitching Using Visible Light: A New Class of Organic Photochromic Molecules, *J. Am. Chem. Soc.*, 2014, **136**, 8169–8172.

18 J. Gemen, J. R. Church, T.-P. Ruoko, N. Durandin, M. J. Białek, M. Weißenfels, M. Feller, M. Kazes, M. Odaybat, V. A. Borin, R. Kalepu, Y. Diskin-Posner, D. Oron, M. J. Fuchter, A. Priimagi, I. Schapiro and R. Klajn, Disequilibrating azobenzenes by visible-light sensitization under confinement, *Science*, 2023, **381**, 1357–1363.

19 G. C. Thaggard, K. C. Park, J. Lim, B. K. P. Maldeni Kankanamalage, J. Haimerl, G. R. Wilson, M. K. McBride, K. L. Forrester, E. R. Adelson, V. S. Arnold, S. T. Wetthasinghe, V. A. Rassolov, M. D. Smith, D. Sosnin, I. Aprahamian, M. Karmakar, S. K. Bag, A. Thakur, M. Zhang, B. Z. Tang, J. A. Castaño, M. N. Chaur, M. M. Lerch, R. A. Fischer, J. Aizenberg, R. Herges, J.-M. Lehn and N. B. Shustova, Breaking the photoswitch speed limit, *Nat. Commun.*, 2023, **14**, 7556.

20 R. Klajn, Spiropyran-based dynamic materials, *Chem. Soc. Rev.*, 2014, **43**, 148–184.

21 J. N. Bull, E. Carrascosa, N. Mallo, M. S. Scholz, G. da Silva, J. E. Beves and E. J. Bieske, Photoswitching an Isolated Donor–Acceptor Stenhouse Adduct, *J. Phys. Chem. Lett.*, 2018, **9**, 665–671.

22 D. E. Williams, C. R. Martin, E. A. Dolgopolova, A. Swifton, D. C. Godfrey, O. A. Ejegbavwo, P. J. Pellechia, M. D. Smith and N. B. Shustova, Flipping the Switch: Fast Photoisomerization in a Confined Environment, *J. Am. Chem. Soc.*, 2018, **140**, 7611–7622.

23 J. Calbo, C. E. Weston, A. J. P. White, H. S. Rzepa, J. Contreras-García and M. J. Fuchter, Tuning Azoheteroarene Photoswitch Performance through Heteroaryl Design, *J. Am. Chem. Soc.*, 2017, **139**, 1261–1274.

24 L.-Q. Zheng, S. Yang, J. Lan, L. Gyr, G. Goubert, H. Qian, I. Aprahamian and R. Zenobi, Solution Phase and Surface Photoisomerization of a Hydrazone Switch with a Long Thermal Half-Life, *J. Am. Chem. Soc.*, 2019, **141**, 17637–17645.

25 A. D. W. Kennedy, I. Sandler, J. Andréasson, J. Ho and J. E. Beves, Visible-Light Photoswitching by Azobenzazoles, *Chem.–Eur. J.*, 2020, **26**, 1103–1110.

26 A. K. Jaiswal, P. Saha, J. Jiang, K. Suzuki, A. Jasny, B. M. Schmidt, S. Maeda, S. Hecht and C.-Y. D. Huang, Accessing a Diverse Set of Functional Red-Light Photoswitches by Selective Copper-Catalyzed Indigo N-Arylation, *J. Am. Chem. Soc.*, 2024, **146**, 21367–21376.
27 J. L. Greenfield, M. A. Gerkman, R. S. L. Gibson, G. G. D. Han and M. J. Fuchter, Efficient Electrocatalytic Switching of Azoheteroarenes in the Condensed Phases, *J. Am. Chem. Soc.*, 2021, **143**, 15250–15257.
28 J. Humphreys, F. Malagreca, P. A. Hume, E. S. Davies, S. P. Argent, T. D. Bradshaw and D. B. Amabilino, Highly electron deficient diketopyrrolopyrroles, *Chem. Commun.*, 2023, **59**, 1613–1616.
29 Z. S. Kean, S. Akbulatov, Y. Tian, R. A. Widenhoefer, R. Boulatov and S. L. Craig, Photomechanical Actuation of Ligand Geometry in Enantioselective Catalysis, *Angew. Chem., Int. Ed.*, 2014, **53**, 14508–14511.
30 B. Shao, H. Qian, Q. Li and I. Aprahamian, Structure Property Analysis of the Solution and Solid-State Properties of Bistable Photochromic Hydrazones, *J. Am. Chem. Soc.*, 2019, **141**, 8364–8371.
31 J. Wang, L. Avram, Y. Diskin-Posner, M. J. Białek, W. Stawski, M. Feller and R. Klajn, Altering the Properties of Spiropyran Switches Using Coordination Cages with Different Symmetries, *J. Am. Chem. Soc.*, 2022, **144**, 21244–21254.
32 M. Samperi, B. Bdiri, C. D. Sleet, R. Markus, A. R. Mallia, L. Pérez-García and D. B. Amabilino, Light-controlled micron-scale molecular motion, *Nat. Chem.*, 2021, **13**, 1200–1206.
33 P. Lentes, P. Frühwirt, H. Freißmuth, W. Moormann, F. Kruse, G. Gescheidt and R. Herges, Photoswitching of Diazocines in Aqueous Media, *J. Org. Chem.*, 2021, **86**, 4355–4360.
34 M. A. Sinnwell and L. R. MacGillivray, Halogen-Bond-Templated [2+2] Photodimerization in the Solid State: Directed Synthesis and Rare Self-Inclusion of a Halogenated Product, *Angew. Chem., Int. Ed.*, 2016, **55**, 3477–3480.
35 J. Usuba, Z. Sun, H. P. Q. Nguyen, C. Raju, K. Schmidt-Rohr and G. G. D. Han, Mechanoactivated amorphization and photopolymerization of styryldipyryliums, *Commun. Mater.*, 2024, **5**, 98.
36 J. Usuba and G. G. D. Han, Photoswitch designs for molecular solar thermal energy storage, *Trends Chem.*, 2023, **5**, 577–580.
37 S. Cho, J. Usuba, S. Chakraborty, X. Li and G. G. D. Han, Solid-state photon energy storage via reversible [2+2] cycloaddition of donor-acceptor styrylpyrylium system, *Chem*, 2023, **9**, 3159–3171.
38 S. Chakraborty, H. P. Q. Nguyen, J. Usuba, J. Y. Choi, Z. Sun, C. Raju, G. Sigelmann, Q. Qiu, S. Cho, S. M. Tenney, K. E. Shulenberger, K. Schmidt-Rohr, J. Park and G. G. D. Han, Self-activated energy release cascade from anthracene-based solid-state molecular solar thermal energy storage systems, *Chem*, 2024, DOI: **10.1016/j.chempr.2024.06.033**.
39 M. A. Gerkman, R. S. L. Gibson, J. Calbo, Y. Shi, M. J. Fuchter and G. G. D. Han, Arylazopyrazoles for Long-Term Thermal Energy Storage and Optically Triggered Heat Release below 0 °C, *J. Am. Chem. Soc.*, 2020, **142**, 8688–8695.
40 Q. Qiu, M. A. Gerkman, Y. Shi and G. G. D. Han, Design of phase-transition molecular solar thermal energy storage compounds: compact molecules with high energy densities, *Chem. Commun.*, 2021, **57**, 9458–9461.
41 A. Gonzalez, M. Odaybat, M. Le, J. L. Greenfield, A. J. P. White, X. Li, M. J. Fuchter and G. G. D. Han, Photocontrolled Energy Storage in Azobispyrazoles with Exceptionally Large Light Penetration Depths, *J. Am. Chem. Soc.*, 2022, **144**, 19430–19436.
42 A. Dreos, Z. Wang, J. Udmark, A. Ström, P. Erhart, K. Börjesson, M. B. Nielsen and K. Moth-Poulsen, Liquid Norbornadiene Photoswitches for Solar Energy Storage, *Adv. Energy Mater.*, 2018, **8**, 1703401.
43 M. Quant, A. Lennartson, A. Dreos, M. Kuisma, P. Erhart, K. Börjesson and K. Moth-Poulsen, Low Molecular Weight Norbornadiene Derivatives for Molecular Solar-Thermal Energy Storage, *Chem.–Eur. J.*, 2016, **22**, 13265–13274.
44 L. E. Gusel'nikov, V. G. Avakyan and S. L. Guselnikov, Hetero-π-systems from 2 + 2 cycloreversion, part 2.1. Ab initio thermochemical study of heterocyclobutanes 2 + 2 cycloreversion to form heteroethenes H2C=X (X=NH, O, SiH2, PH, S), *Heteroat. Chem.*, 2007, **18**, 704–720.
45 R. O. Kan and R. L. Furey, Photochemical formation of 1,3-diazetidines, *J. Am. Chem. Soc.*, 1968, **90**, 1666–1667.
46 B. B. Lohray, V. B. Lohray and B. K. Srivastava, in *Comprehensive Heterocyclic Chemistry III*, ed. A. R. Katritzky, C. A. Ramsden, E. F. V. Scriven and R. J. K. Taylor, Elsevier, Oxford, 2008, pp. 623–687.
47 J. Roussilhe, J. Roussilhe, E. Fargin, A. Lopez, B. Despax and N. Paillous, Photochemical behavior of 2-phenylbenzoxazole. Synthesis of 1,3-diazetidine via the intermolecular [2.pi. + 2.pi.] cycloaddition of two carbon-nitrogen double bonds, *J. Org. Chem.*, 1983, **48**, 3736–3741.
48 J. Roussilhe, B. Despax, A. Lopez and N. Paillous, Photodimerization of 2-phenylbenzoxazole and its acid-catalysed reversion as a new system for light energy conversion, *J. Chem. Soc., Chem. Commun.*, 1982, 380–381.
49 M. D'Auria, A. Guarnaccio, R. Racioppi, S. Stoia and L. Emanuele, in *Photochemistry of Heterocycles*, ed. M. D'Auria, A. Guarnaccio, R. Racioppi, S. Stoia and L. Emanuele, Elsevier, 2023, pp. 219–296.
50 P. Molina, M. Alajarin, C. Lopez-Leonardo and J. Elguero, Four-membered Heterocyclic Rings from Iminophosphoranes. Preparation and reactivity of 2,4-diimino-1,3-diazetidines and related compounds, *J. Prakt. Chem./Chem.-Ztg.*, 1993, **335**, 305–315.
51 N. Kaur, in *4-Membered Heterocycle Synthesis*, ed. N. Kaur, Elsevier, 2023, vol. 5, pp. 1–42.
52 S. Fery-Forgues and N. Paillous, Photodehalogenation and photodimerization of 2-(4-halophenyl)benzoxazoles. Dependence of the mechanism on the nature of the halogen atom, *J. Org. Chem.*, 1986, **51**, 672–677.

53 N. Paillous, S. F. Forgues, J. Jaud and J. Devillers, [2 + 2] Cycloaddition of two C=N double bonds. First structural evidence for head-to-tail photodimerization in the 2-phenylbenzoxazole series, *J. Chem. Soc., Chem. Commun.*, 1987, 578–579.

54 D. Lawrenz, S. Mohr and B. Wendländer, Formation of 1,3-diazetidines via C–N dimerization of 4-cycloalkylideneoxazol-5(4H)-ones in the solid state, *J. Chem. Soc., Chem. Commun.*, 1984, 863–865.

55 C. Carayon and S. Fery-Forgues, 2-Phenylbenzoxazole derivatives: a family of robust emitters of solid-state fluorescence, *Photochem. Photobiol. Sci.*, 2017, **16**, 1020–1035.

56 H. Bouas-Laurent, A. Castellan, J.-P. Desvergne and R. Lapouyade, Photodimerization of anthracenes in fluid solutions: (part 2) mechanistic aspects of the photocycloaddition and of the photochemical and thermal cleavage, *Chem. Soc. Rev.*, 2001, **30**, 248–263.

57 S. B. Kim, D. H. Kim and H. Y. Bae, "On-Water" accelerated dearomative cycloaddition via aquaphotocatalysis, *Nat. Commun.*, 2024, **15**, 3876.

58 C. Raju, G. R. Ramteke, K. V. J. Jose and K. M. Sureshan, Cascading Effect of Large Molecular Motion in Crystals: A Topotactic Polymorphic Transition Paves the Way to Topochemical Polymerization, *J. Am. Chem. Soc.*, 2023, **145**, 9607–9616.

59 J. B. Benedict and P. Coppens, Kinetics of the Single-Crystal to Single-Crystal Two-Photon Photodimerization of α-trans-Cinnamic Acid to α-Truxillic Acid, *J. Phys. Chem. A*, 2009, **113**, 3116–3120.

60 K. Morimoto, D. Kitagawa, F. Tong, K. Chalek, L. J. Mueller, C. J. Bardeen and S. Kobatake, Correlating Reaction Dynamics and Size Change during the Photomechanical Transformation of 9-Methylanthracene Single Crystals, *Angew. Chem., Int. Ed.*, 2022, **61**, e202114089.

61 S. Kataoka, D. Kitagawa, H. Sotome, S. Ito, H. Miyasaka, C. J. Bardeen and S. Kobatake, Relationship between spatially heterogeneous reaction dynamics and photochemical kinetics in single crystals of anthracene derivatives, *Chem. Sci.*, 2024, **15**, 13421–13428.

62 G. C. George III and K. M. Hutchins, Solid-State [4+4] Cycloaddition and Cycloreversion with Use of Unpaired Hydrogen-Bond Donors to Achieve Solvatomorphism and Stabilization, *Chem.–Eur. J.*, 2023, **29**, e202302482.

63 P. v. R. Schleyer, C. Maerker, A. Dransfeld, H. Jiao and N. J. R. van Eikema Hommes, Nucleus-Independent Chemical Shifts: A Simple and Efficient Aromaticity Probe, *J. Am. Chem. Soc.*, 1996, **118**, 6317–6318.